Chemistry—Methods

Research Article
doi.org/10.1002/cmtd.202500157

Chemistry Europe
European Chemical Societies Publishing

www.chemistrymethods.org

Selective H^+ Exchange for External Surface of Zeolites to Elucidate the Role of External Acid Sites of Zeolite in Polyolefin Cracking

Ryuga Nakai,* Shinya Kokuryo, Koji Miyake,* Yoshiki Murata, Yoshiaki Uchida, Atsushi Mizusawa, Tadashi Kubo, and Norikazu Nishiyama

Zeolites are widely studied as promising catalysts for the chemical recycling of plastics due to their inherent microporosity and shape-selective properties. The accessibility of polymer chains to internal acid sites is limited, and initial reactions are supposed to occur near the external surface. A deeper understanding of the role of external acid sites is required to optimize the structure and morphology of the zeolites. In this study, a novel ZSM-5 zeolite catalyst with Brønsted acid sites selectively localized only on the external surface (ZSM-5-SA) is synthesized via selective ion exchange using bulky tetrapropylammonium ions, followed by calcination. Catalytic testing of low- and high-density polyethylene revealed that the initial degradation is mainly triggered at Brønsted acid sites located on the external surface and near-surface internal regions. Once protonated, the polymer chains undergo β-scission, leading to similar product distributions regardless of the acid site density. These findings highlight that a small number of spatially accessible acid sites can effectively initiate and propagate the cracking reaction. These findings establish a direct link between the acid site location and reaction pathway and offer a rational design principle for advanced zeolite catalysts tailored for polymer cracking and chemical upcycling.

1. Introduction

In recent years, many efforts have been made toward achieving a sustainable society, and various solutions have been explored internationally. Among them, chemical recycling can realize the conversion of waste plastics into raw materials, and especially, catalytic cracking of plastics using zeolite catalysts is one of the important research topics.[1–7]

Zeolites are crystalline microporous aluminosilicates with tetrahedral TO_4 units centered on metal elements. Zeolites are mainly composed of SiO_2; the partial substitution of Si^{4+} with Al^{3+} causes charge imbalances, which are compensated by counter cations in the framework. The counter cations in zeolites can be readily exchanged with other cations. Among these, the introduction of protons, typically achieved through calcination of NH_4^+-type zeolites, leads to H^+-type zeolites, which exhibit Brønsted acidity. Because of these physicochemical properties, zeolites are considered suitable for the catalytic cracking of plastics.[8–15]

Due to the large molecular size of polymers, it has been proposed that catalytic cracking initially occurs at Brønsted acid sites on the external surface of zeolites, where polymers can physically access the active sites. Several studies have supported this idea by demonstrating the importance of external acid sites in initiating the degradation of polymers.[16–19] In our previous study, we prepared ZSM-5/silicalite-1 core–shell structured zeolites with varying shell thicknesses to investigate this hypothesis.[20] The results revealed that not only the external acid sites but also internal acid sites located near the surface contributed to the initial stages of low-density polyethylene (LDPE) cracking.

However, the role of internal acid sites, especially those located deep within the micropores, remains poorly understood. While some studies have suggested that smaller fragments formed on the external surface can further diffuse into the micropores and undergo secondary cracking, this mechanism has not been directly proven by experiments.[21–24] Our findings indicated that even shallow internal acid sites could participate in early-stage reactions; however, the contribution of deeper internal acid sites is still unclear. The catalytic degradation of polyolefins is strongly affected by both the framework structure and the spatial distribution of acid sites; however, decoupling these effects is

R. Nakai, S. Kokuryo, K. Miyake, Y. Murata, Y. Uchida, N. Nishiyama
Graduate School of Engineering Science
Division of Chemical Engineering
The University of Osaka
1–3 Machikaneyama, Toyonaka, Osaka 560–8531, Japan
E-mail: r.nakai@cheng.es.osaka-u.ac.jp
k.miyake.es@osaka-u.ac.jp

K. Miyake, N. Nishiyama
Innovative Catalysis Science Division
Institute for Open and Transdisciplinary Research Initiatives (ICS-OTRI)
The University of Osaka
Suita, Osaka 565–0871, Japan

A. Mizusawa, T. Kubo
AC Biode Co., Ltd.
498–6 Iwakura Hanazono, Sakyo, Kyoto 606–0024, Japan

Supporting information for this article is available on the WWW under https://doi.org/10.1002/cmtd.202500157

Research Article
doi.org/10.1002/cmtd.202500157
Chemistry Europe
European Chemical Societies Publishing

challenging. Yi Wang et al. systematically investigated the influence of pore structure on product distribution during polyolefin cracking and demonstrated that differences in zeolitic architecture significantly affect reaction outcomes.[25] This study highlighted the importance of physical structure, but also pointed to the difficulty of separating structural effects from those of acidity. Lingfeng Yu et al. reported that hierarchical ZSM-5 zeolites containing mesopores exhibit enhanced activity for LDPE cracking, emphasizing the positive impact of mesoporosity on diffusion and reactivity.[26] However, changes in porosity are often accompanied by variations in acid strength and density, making it challenging to attribute the catalytic improvement solely to the mesostructure. A. Coelho et al. addressed the contribution of internal acid sites by modulating the Brønsted acidity of ZSM-5 through Na^+ ion exchange. They proposed that the observed differences in cracking temperature of polyethylene were primarily due to the internal acidity, as most acid sites in ZSM-5 are located within micropores.[27] These studies have significantly contributed to the field; however, a common limitation persists: the difficulty in decoupling the effects of internal and external acid sites, especially since procedures such as ion exchange may unintentionally alter both sites. In this study, we aimed to synthesize zeolites with acid sites only on the external surface and compare them with conventional zeolite catalysts to reveal the role of internal acid sites and the physical effects on the pore structure in catalytic cracking reactions.

Scheme 1 illustrates a novel method for controlling acid sites via ion exchange. In detail, we synthesized Na^+-type ZSM-5 without Brønsted acidity, and then performed an ion exchange using tetrapropylammonium bromide (TPABr). Only Na^+ ions on the external surface of ZSM-5 could be exchanged for tetrapropylammonium (TPA^+) ions because the molecular size of TPA^+ ions is larger than the micropore size of ZSM-5, and the TPA^+ ions on the external surface can be transformed into H^+ via calcination.[28–32] Thus, zeolites with Brønsted acid only on the external surface can be synthesized by the sequential processes of TPA^+ exchange and calcination using Na^+-type ZSM-5 without Brønsted acidity. The catalytic reactions using the ZSM-5 with acidity only on the external surface are expected to give some evidence on the role of each of the inner and external acid sites for polyethylene cracking activity (cracking temperature, product distributions, and coking inhibition).

2. Results and Discussion

X-ray diffraction (XRD) patterns of all samples displayed sharp and characteristic MFI-type peaks, as shown in **Figure 1**a, indicating that the ion-exchange treatment did not affect the structural integrity of the zeolite framework. The results of the energy-dispersive X-ray (EDX) analysis and N_2 adsorption measurements are summarized in **Table 1**. The EDX analysis showed that the Si/Al ratios remained almost constant across all samples, including Na/ZSM-5, H/ZSM-5, and ZSM-5-SA, indicating that the ion-exchange processes did not affect the overall composition or framework integrity. This structural and compositional stability was further supported by the N_2 adsorption measurements (Figure S1, Supporting Information), which showed comparable specific surface areas and pore volumes for all samples. These results indicate that the microporous properties and external surface areas were not significantly affected, implying that the morphology and particle size remained essentially unchanged throughout the ion-exchange modifications. Furthermore, no Na^+ was detectable by the EDX analysis of H/ZSM-5, whereas ZSM-5-SA exhibited a slightly lower Na/Al ratio than Na/ZSM-5. These results show that most of the Na^+ ions in Na/ZSM-5 did not undergo ion exchange. Although EDX elemental mapping was conducted, no discernible differences were detected between Na/ZSM-5 and ZSM-5-SA, as shown in Figure S2, Supporting Information. The X-ray photoelectron spectroscopy (XPS) spectra on Na 1s for each sample are shown in Figure 1b. XPS is generally capable of detecting elements within a few nanometers from the sample surface, allowing evaluation of Na near the external surface. As a result, ZSM-5-SA exhibited less than half the Na content of Na/ZSM-5. These results suggest that H^+ largely replaced Na^+ near the external surface of ZSM-5-SA, indicating selective introduction of Brønsted acid sites on the external surface. If Na^+ and H^+ were randomly distributed

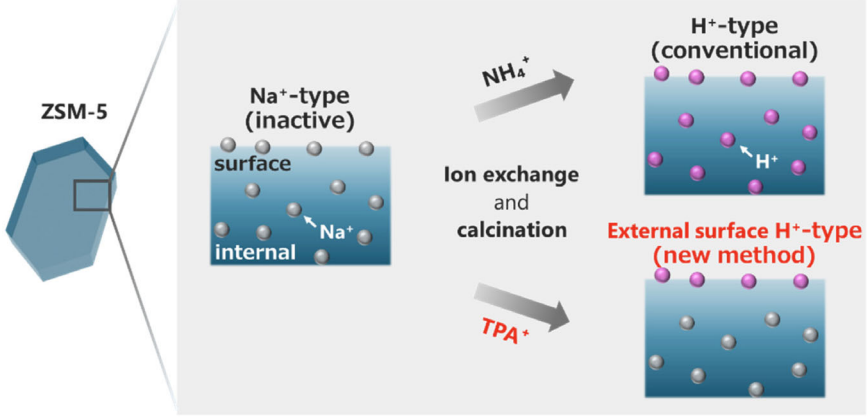

Scheme 1. Control of acid sites via ion exchange.

Research Article
doi.org/10.1002/cmtd.202500157
Chemistry Europe
European Chemical Societies Publishing

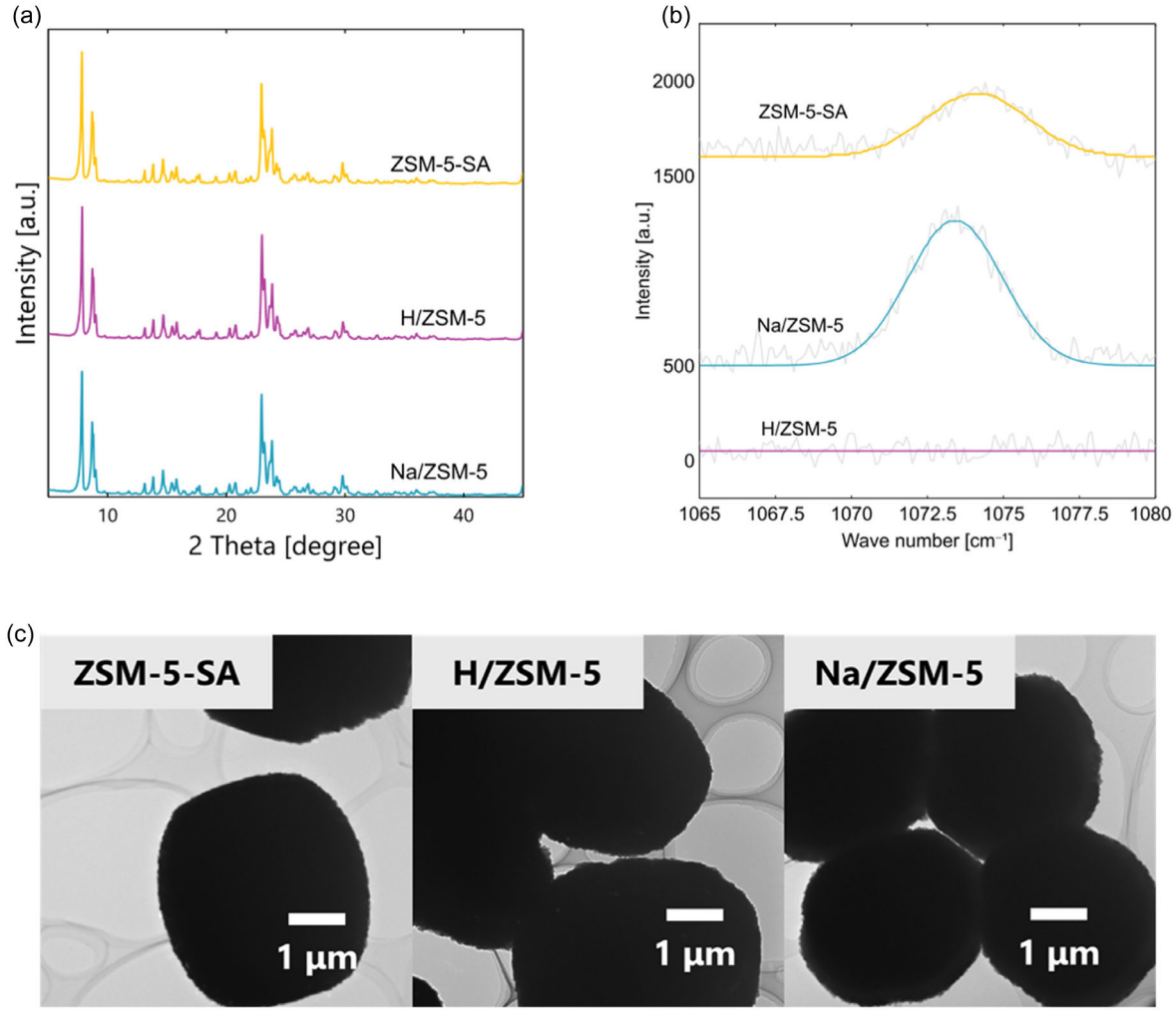

Figure 1. a) XRD patterns, b) XPS spectra on Na 1s, and c) TEM images of Na/ZSM-5, H/ZSM-5, and ZSM-5-SA.

Table 1. Physicochemical properties of Na/ZSM-5, H/ZSM-5, and ZSM-5-SA.

	Si/Al [-]	Na/Al [-]	S_{BET} [$m^2 g^{-1}$]	S_{ext} [$m^2 g^{-1}$]	V_{micro} [$cm^3 g^{-1}$]
ZSM-5-SA	30.6	0.943	338.9	20.38	0.151
H/ZSM-5	27.4	–	363.7	12.35	0.177
Na/ZSM-5	29.9	1.07	307.2	15.05	0.141

throughout the zeolite framework, the Na content detected by XPS in ZSM-5-SA would be similar to that in Na/ZSM-5. Therefore, these results collectively indicate that the synthesized ZSM-5-SA possesses Brønsted acid sites predominantly on the external surface. The transmission electron microscopy (TEM) images of the samples are shown in Figure 1c. All zeolite samples retained a uniform particle morphology with sizes of ≈3–4 µm, suggesting that the ion-exchange steps did not affect their morphology or particle dimensions. To investigate the chemical state of aluminum, ^{27}Al MAS nuclear magnetic resonance (NMR) measurements were performed, as shown in Figure S3, Supporting Information. All spectra exhibited a pronounced peak at ≈54 ppm, corresponding to tetrahedrally coordinated framework aluminum. The intensity of this peak was largely consistent across the samples, indicating that the coordination state of aluminum was well preserved under the applied conditions.[13]

The NH_3-TPD profiles of the three samples are shown in **Figure 2**a. H/ZSM-5 exhibited two distinct desorption peaks: a weak acid site (α) peak at ≈230 °C, and a strong acid site (γ) peak near 450 °C. In contrast, Na/ZSM-5 exhibited a weak acid peak (α) at ≈230 °C and a medium-strength acid site (β) peak at ≈290 °C, whereas no significant γ peak was observed. A similar profile was obtained for ZSM-5-SA, which displayed both α and β peaks comparable to those observed for Na/ZSM-5.[33] The β peaks observed in Na/ZSM-5 and ZSM-5-SA are presumed to originate from Al sites associated with Na^+ ions, whereas the γ peak in H/ZSM-5 is generally attributed to Brønsted acid sites linked to the framework Si–OH–Al groups.[34–36] These findings indicate that the Brønsted acidity of ZSM-5-SA is significantly lower than that of H/ZSM-5, implying that the Brønsted acid sites are localized exclusively on the external surface of the ZSM-5-SA sample.

The distribution of Brønsted acid sites on the external surface of ZSM-5 was evaluated by fourier transform infrared

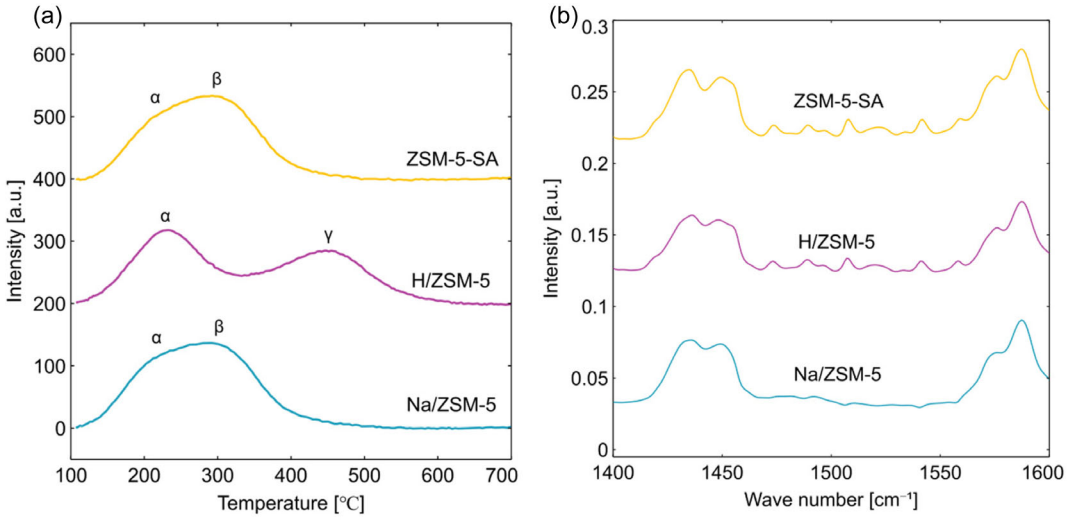

Figure 2. a) NH_3-TPD profiles and b) FT-IR spectra of adsorbed pyridine on Na/ZSM-5, H/ZSM-5, and ZSM-5-SA.

spectrometer (FT-IR) spectroscopy using pyridine as a probe molecule.[37–39] Due to its kinetic diameter (0.57 nm),[40] which is comparable to the pore opening of ZSM-5 (0.51–0.56 nm),[41] pyridine is sterically hindered from diffusing into the internal micropores. Consequently, under ambient adsorption conditions, pyridine is expected to interact primarily with the acid sites located on the external surface, thereby enabling surface-specific acidity analysis. Figure 2b displays the FT-IR spectra of pyridine-adsorbed Na/ZSM-5, H/ZSM-5, and ZSM-5-SA. In the case of H/ZSM-5, a distinct absorption band at ≈1545 cm^{-1} was observed, corresponding to pyridine coordinated to the Brønsted acid sites ($Py–H^+$). This band is characteristic of protons associated with bridging hydroxyl groups (Si–OH–Al) and confirms the presence of strong Brønsted acid sites accessible to pyridine molecules. Notably, a band of comparable intensity appeared at the same wavenumber in the spectrum of ZSM-5-SA, suggesting that this sample also contains Brønsted acid sites exposed on its external surface. In contrast, no such peak was detected in Na/ZSM-5, indicating the absence of protons in this fully Na^+-exchanged sample. The similar intensity of the band at 1545 cm^{-1} in both H/ZSM-5 and ZSM-5-SA implies that the number of Brønsted acid sites on the external surface of ZSM-5-SA is nearly equivalent to that of H/ZSM-5. Combined with the absence of this band in Na/ZSM-5, it can be concluded that the observed Brønsted acidity in ZSM-5-SA originates solely from the external surface, and that pyridine did not penetrate the internal pore system. In addition, Figure S4, Supporting Information shows the FT-IR spectra obtained after repeated pyridine adsorption–desorption cycles at 200 °C for H/ZSM-5 and ZSM-5-SA. In all samples, a band attributable to pyridine adsorbed on Brønsted acid sites was observed at ≈1545 cm^{-1}. The intensities of this band were almost identical for H/ZSM-5 (first) and ZSM-5-SA (first). In the second and third adsorption cycles, the peak intensity increased compared to that in the first adsorption cycle; however, the intensities remained comparable between H/ZSM-5 and ZSM-5-SA. These results indicate that, after removal of physically adsorbed species such as water, the amounts of Brønsted acid sites located on the external surface were nearly the same for both samples. If pyridine molecules had diffused into the internal pores of ZSM-5, the Brønsted acid band of H/ZSM-5 would have shown a much stronger intensity. Therefore, under the present measurement conditions, pyridine adsorption is considered to be restricted to the external surface, enabling evaluation of only the external Brønsted acid sites. The temperature dependence of pyridine diffusion further supports this interpretation. Bludau et al. systematically investigated the sorption and diffusion behavior of pyridine in H-ZSM-5 and reported that steady-state intracrystalline diffusion occurs at elevated temperatures around 300 °C.[42] Considering that the kinetic diameter of pyridine is nearly identical to the pore aperture of the MFI framework, substantial thermal energy is required for pyridine to enter the micropores of the MFI framework. Under the present experimental conditions (150 °C and 200 °C), pyridine is therefore expected to adsorb predominantly on Brønsted acid sites located on or near the external surface. This initial adsorption effectively limits further diffusion into the internal pores. Consistently, the nearly identical intensities of the 1545 cm^{-1} band observed for H/ZSM-5 and ZSM-5-SA across multiple adsorption cycles indicate the absence of pyridine diffusion into the internal pore system. Additional support for the preferential interaction of pyridine with external acid sites is provided by XPS measurements. Specifically, Na 1s XPS selectively probes sodium species near the external surface, and the observed differences between Na/ZSM-5 and ZSM-5-SA confirm that ion-exchange and surface modification occurred primarily on the external surface. These XPS results are in agreement with the FT-IR observations, reinforcing the conclusion that pyridine adsorption under these conditions is largely restricted to externally accessible Brønsted acid sites. Taken together, literature evidence, FT-IR data, and XPS analysis indicate that, under the present mild adsorption conditions, the

Research Article
doi.org/10.1002/cmtd.202500157
Chemistry Europe
European Chemical Societies Publishing

measured Brønsted acidity predominantly reflects the external surface, enabling a selective and reliable evaluation of external acid sites.

These findings strongly support the hypothesis that H^+ ions were selectively introduced to the external surface of ZSM-5-SA without affecting the internal Na^+ cationic framework. This conclusion is further supported by the NH_3-TPD results. While H/ZSM-5 exhibited both low- and high-temperature desorption peaks, corresponding to weak and strong Brønsted acid sites, ZSM-5-SA displayed only a significantly weaker high-temperature peak, reflecting a substantial reduction in the total amount of Brønsted acid sites. FT-IR and NH_3-TPD results confirmed that ZSM-5-SA possessed Brønsted acid sites exclusively on its external surface, demonstrating the successful synthesis of a spatially acid-controlled zeolite catalyst.

Figure 3a shows the LDPE degradation profiles obtained by thermogravimetric (TG) analysis using Na/ZSM-5, H/ZSM-5, and ZSM-5-SA. Na/ZSM-5 exhibited virtually no catalytic activity, as indicated by the decomposition curve, which was nearly identical to that observed under noncatalytic conditions. In contrast, H/ZSM-5 significantly promoted LDPE degradation, with the main decomposition temperature reduced by ≈130 °C compared to both Na/ZSM-5 and the noncatalytic reference. This pronounced shift toward lower temperatures indicates the high catalytic activity of H/ZSM-5, which is attributable to the presence of abundant Brønsted acid sites distributed throughout the zeolite framework. ZSM-5-SA exhibited moderate activity, with a slight decrease in the decomposition temperature relative to Na/ZSM-5, suggesting that the presence of Brønsted acid sites only on the external surface contributes partially to the polymer cracking reaction. The difference in the decomposition onset temperatures between H/ZSM-5 and ZSM-5-SA highlights the contribution of internal acid sites to polyolefin cracking. Given the large molecular size of LDPE, it is unlikely that entire polymer chains can enter the micropores of ZSM-5. However, segments of the polymer (particularly the chain ends or branched portions) may be able to reach acid sites located just inside the pore mouths (**Scheme 2**). Therefore, it is reasonable to assume that the acid sites in the near-surface internal region, in addition to those on the external surface, play a role in initiating the degradation process. This interpretation is further supported by previous studies, such as the work by Tsubota et al., in which core–shell structured

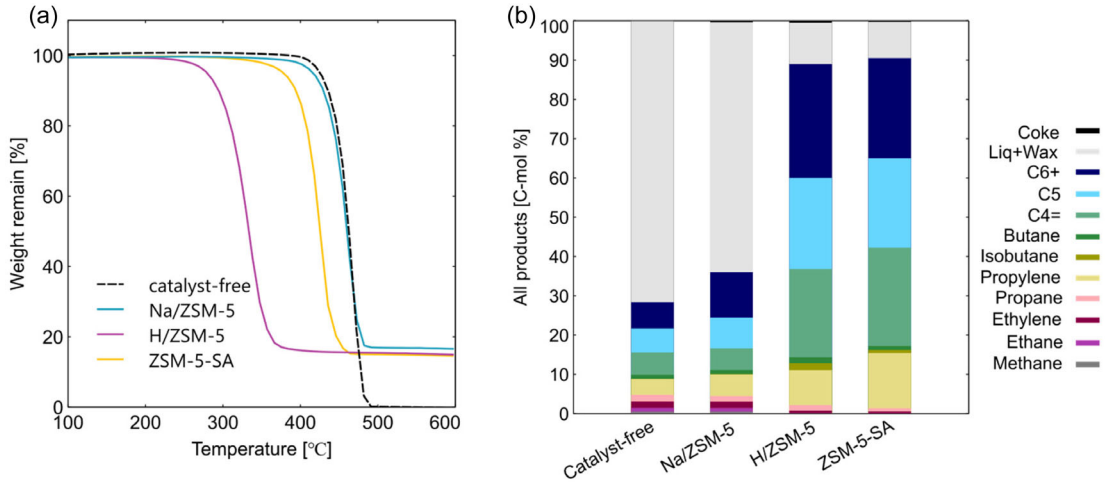

Figure 3. a) TG curves obtained during catalytic cracking of LDPE and b) product distributions over LDPE cracking with Na/ZSM-5, H/ZSM-5, and ZSM-5-SA.

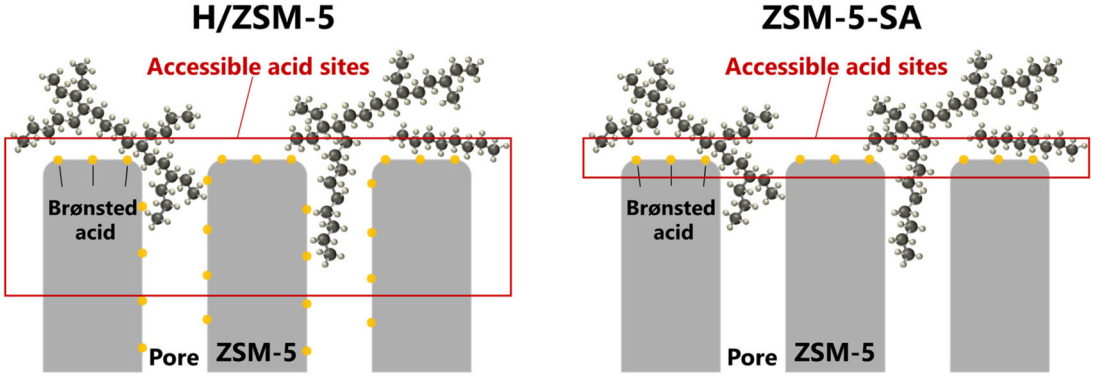

Scheme 2. Acid sites accessible to LDPE in the initial stage of cracking.

ZSM-5 was investigated with varying shell thicknesses.[20] They demonstrated that increasing the shell thickness, which reduces the accessibility of near-surface acid sites, leads to a decline in degradation activity. This supports the notion that spatially accessible acid sites near the pore entrances are critical for initiating polyolefin cracking. The number of such accessible sites is expected to be higher in H/ZSM-5 than in ZSM-5-SA, accounting for the observed difference in the degradation onset temperatures. Taken together, these results suggest that the degradation temperature is governed not only by the total number of Brønsted acid sites but also by their spatial accessibility, specifically, whether they are located within the range accessible by bulky polymer chains.

Figure 3b shows the product distributions obtained from the catalytic cracking of LDPE over Na/ZSM-5, H/ZSM-5, and ZSM-5-SA, as analyzed by gas chromatography. In the case of Na/ZSM-5, the product distribution was similar to that obtained under non-catalytic conditions, with a significant proportion of liquid-phase products. This result confirms the absence of catalytic activity in Na/ZSM-5 due to the lack of active acid sites. In contrast, H/ZSM-5 exhibited high catalytic activity, yielding ≈90% gaseous products composed mainly of low-carbon hydrocarbons. Remarkably, ZSM-5-SA, which contains Brønsted acid sites exclusively on its external surface, also achieved a gas yield of ≈90%, which is comparable to that of H/ZSM-5. Furthermore, the composition of the gaseous products obtained from ZSM-5-SA closely resembled that of H/ZSM-5. These findings indicate that the presence of Brønsted acid sites on the external surface alone is sufficient to facilitate extensive LDPE cracking and produce a product distribution similar to that of a catalyst possessing acid sites throughout the entire framework.

Moreover, a slightly higher yield of propane was observed in the product stream from H/ZSM-5 compared to ZSM-5-SA, indicating more pronounced hydrogen transfer reactions. These reactions, facilitated by internal Brønsted acid sites, convert olefins into saturated hydrocarbons such as propane. Hydrogen transfer is also associated with coke formation through secondary reactions, including cyclization and aromatization.[43–45] The decomposition profiles of the coke deposits obtained by TG analysis, as well as their physical appearance, showed noticeable differences in H/ZSM-5 (Figure S5, Supporting Information). During the catalytic cracking of polyethylene over H/ZSM-5, olefins and aromatics formed as intermediates undergo dehydrogenation and condensation within the zeolite pores, ultimately leading to the formation of coke precursors. Brønsted acid sites are known to promote these processes by facilitating both the initial cracking and subsequent aromatization step.[46–48] Therefore, although internal acid sites enhance the cracking efficiency, they may also increase the tendency for coke formation during LDPE cracking reactions.

In addition, LDPE cracking progresses via a well-established Brønsted acid–mediated carbocation (carbenium ion) mechanism. Protonation of the polymer chain leads to the formation of a carbenium ion, which then undergoes β-scission (breaking of a C—C bond adjacent to the carbenium center), yielding smaller hydrocarbon fragments such as light alkanes and olefins.[49,50] While TG analysis (Figure 3a) suggests that LDPE cracking may be initiated at Brønsted acid sites located on or near the external surface of the zeolite, the gas chromatography results (Figure 3b) further imply that the subsequent degradation is predominantly governed by β-scission of the polymer backbone. In particular, the high gas yield and the similarity in product composition between ZSM-5-SA and H/ZSM-5, despite the former having a much lower acid site density, indicate that once the polymer is activated by protonation, chain cleavage proceeds mainly through β-scission mechanisms. This implies that a limited number of accessible acid sites can effectively initiate the reaction, after which the fragmentation of polymer chains becomes the dominant pathway. While MFI-type zeolites are generally recognized for promoting the formation of aromatic compounds during polyethylene (PE) cracking, the catalytic performance strongly depends on the Si/Al ratio. In this study, the ZSM-5 samples possessed relatively high Si/Al ratios, corresponding to lower acid site densities and consequently reduced aromatization activity. This trend is supported by the work of Wenjie Wang et al., who investigated PE cracking over ZSM-5 with SiO_2/Al_2O_3 ratios of 25, 38, and 7.[51] Their results showed that the catalyst with $SiO_2/Al_2O_3 \approx 38$ (Si/Al $\approx$ 19) exhibited the highest aromatic yields. Because the Si/Al ratios of the ZSM-5 materials in this study were higher than this optimal value, significant BTX formation was not expected. The reaction conditions used here further limit aromatization. Compared with the conditions reported in the literature that are favorable for aromatic production (e.g., 500 °C, LDPE:ZSM-5 = 1:6), the present conditions involve a much lower catalyst-to-polymer ratio (LDPE:ZSM-5 = 4:1), which suppresses the progression of reactions leading to BTX. Moreover, Wenjie Wang et al. showed that noble metals such as Pt were required to substantially increase aromatic yields, highlighting the intrinsic difficulty of achieving high aromatization performance with ZSM-5 alone. As the catalysts used here do not contain aromatization-promoting elements such as Zn or Ga, significant BTX formation is unlikely. Taken together, the relatively high Si/Al ratio, catalyst-limited reaction conditions, and absence of metal promoters resulted in minimal aromatic production. This provides a consistent explanation for why both ZSM-5-SA and H/ZSM-5 exhibited product distributions dominated by gaseous components (C_6^+) rather than individual BTX compounds, despite the differences in their acid site densities.

To further validate the generality of these findings, similar catalytic cracking experiments were conducted using high-density polyethylene (HDPE) as the feedstock (Figure S6, Supporting Information). The trends observed for HDPE closely paralleled those obtained for LDPE. Specifically, Na/ZSM-5 exhibited minimal catalytic activity similarly, whereas both ZSM-5-SA and H/ZSM-5 produced high yields of gaseous products with comparable distributions. Moreover, both the decomposition profile of the coke and its appearance were similar to those observed in the case of LDPE cracking (Figure S7, Supporting Information).

However, a closer examination of the initial decomposition stage in the HDPE cracking profile over H/ZSM-5 revealed a slightly lower slope compared to that of LDPE, indicating reduced cracking activity. This difference is likely attributable to the

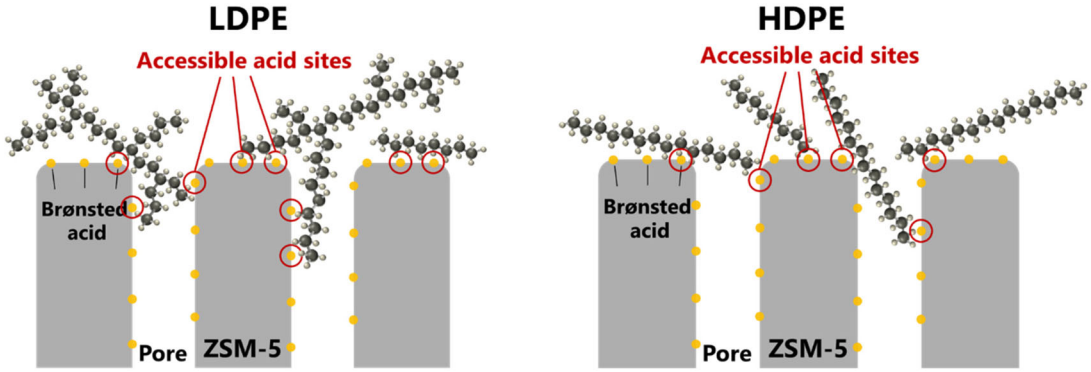

Scheme 3. Acid sites accessible to LDPE and HDPE in the initial stage of cracking.

structural differences between HDPE and LDPE. LDPE possesses a highly branched polymer architecture, which enables its side chains to more readily interact with near-surface internal Brønsted acid sites after initial adsorption on the external surface. In contrast, HDPE features a more linear structure with fewer branches, limiting its ability to access these internal sites. In such cases, the linear polymer chains must insert themselves into the micropores, much like a needle penetrating a narrow channel, to reach the acid sites located just beneath the surface (**Scheme 3**). These structural differences between the polymers are likely to account for the observed variation in initial cracking behavior. These results serve to reinforce the conclusions drawn from the TG analysis, providing additional support for the notion that the initial stage of polymer decomposition is predominantly governed by Brønsted acid sites located on the external surface and in the near-surface internal regions of the zeolite.

To investigate the influence of protons distributed within the micropores, a ZSM-5 sample containing a trace amount of H^+ was prepared by ion-exchanging Na/ZSM-5 with a very dilute aqueous NH_4Cl solution. This sample is hereafter referred to as ZSM-5-WA. As shown in Figure S8a, Supporting Information, the NH_3-TPD profile confirmed that the Brønsted acidity of ZSM-5-WA was negligible, which is similar to that of ZSM-5-SA. Moreover, the FT-IR spectra obtained using pyridine adsorption (after degassing at 200 °C), as shown in Figure S8b, Supporting Information, exhibited a small but distinct band attributed to pyridine adsorbed on Brønsted acid sites, comparable in shape to that of ZSM-5-SA, although slightly weaker in intensity than that of H/ZSM-5 and ZSM-5-SA. The TG analysis of the polymer cracking activity, shown in Figure S8c, Supporting Information, revealed that ZSM-5-WA exhibited degradation activity comparable to that of ZSM-5-SA. Furthermore, as illustrated in Figure S8d, Supporting Information, the distribution of the degradation products indicated a slight increase (≈5%) in liquid products compared to H/ZSM-5 and ZSM-5-SA. These results suggest that, due to the low concentration of the NH_4Cl solution, ion exchange with Na^+ likely occurred preferentially near the external surface of the crystals, where diffusion of NH_4^+ was relatively less hindered. Consequently, ZSM-5-WA exhibited acidity and catalytic behavior similar to those of ZSM-5-SA. Although this interpretation remains tentative due to the limited precision of quantitative acid-site analysis, such a mechanism is plausible. Importantly, this study is the first to reveal that even when the amount of Brønsted acid sites in ZSM-5 is significantly reduced compared to that in conventional samples, the polyolefin cracking reaction still proceeds effectively, producing gaseous products as the dominant fraction after cracking. The results of this study indicate that the polyolefin cracking activity is primarily determined by the amount of Brønsted acid sites accessible to the polymer chains. Furthermore, the findings demonstrate that when acid sites are present at accessible positions, the cracking reaction proceeds efficiently, even if the total number of acid sites in the zeolite is significantly reduced. Based on these insights, it can be anticipated that zeolite catalysts in which a sufficient number of acid sites are selectively introduced only at polymer-accessible positions could be synthesized. Such catalysts would be expected to exhibit degradation activity and product distributions comparable to those of conventional zeolites containing acid sites throughout the framework, while simultaneously suppressing coke formation within the internal pores, thereby extending catalyst lifetime. The precise ion-exchange strategies developed in this study provide a foundation for synthesizing such catalysts, and further control over the side-chain length of the tetrapropylammonium (TPA^+) structure is expected to facilitate selective incorporation of acid sites at the desired positions.

3. Conclusion

In this study, we developed a novel ZSM-5 zeolite catalyst in which Brønsted acid sites were selectively introduced exclusively on the external surface using a spatially controlled ion-exchange technique. This design enabled a clear separation of internal and external acidity, thereby allowing for a systematic investigation into their individual contributions to the catalytic cracking of polyolefins. The catalytic performance testing revealed that the initial stage of LDPE degradation was mainly triggered by Brønsted acid sites located on the external surface and near-surface internal regions, as suggested by TG analysis. Furthermore, GC results revealed that, once protonated, the polymer predominantly undergoes β-scission, leading to similar product distributions regardless of the total acid site density. These findings indicate

that a small number of spatially accessible acid sites are sufficient to initiate efficient cracking and govern the product selectivity. Such mechanistic insights provide a foundation for the rational design of next-generation solid acid catalysts tailored for specific polymer conversion processes, with implications for both sustainable plastic waste management and the development of advanced hydrocarbon synthesis platforms.

4. Experimental Section

Catalytic Preparation: Synthesis of Na^+-Type Zeolite

Chemical reagents were tetraethyl orthosilicate (TEOS, FUJIFILM Wako Pure Chemical Co.), $Al(NO_3)_3{\cdot}9H_2O$ (FUJIFILM Wako Pure Chemical Co.), Tetrapropylammonium bromide (TPABr, FUJIFILM Wako Pure Chemical Co.), and 4 mol L^{-1} NaOH aqueous solution (FUJIFILM Wako Pure Chemical Co.). In a synthesis procedure, the molar composition of the precursor solution was set to 1.5 SiO_2(TEOS) : 0.5 NaOH : 0.8 TPABr : 120 H_2O. The Al source was added to the solution at a Si/Al ratio of 40. The precursor solution was then stirred at room temperature for 24 h and then transferred to an autoclave and heated for 24 h at 180 °C under static conditions and autogenous pressure. The solid product was separated by centrifugation, and washed with deionized water 3 times. The wet powder was dried overnight at 90 °C and then calcined in air at 550 °C for 5 h to remove the structure-directing agent. The resultant Na^+-type ZSM-5 was ion exchanged with a saturated NaCl solution for 20 h on a hot stirrer at 180 °C to remove the slight remaining Brønsted acid. The powder was then separated by centrifugation. Then, the same procedures of washing, drying, and calcination were performed as mentioned above. This sample was named "Na/ZSM-5".

Synthesis of Selective H^+-Exchange Zeolite on External Surface and H^+-Type Zeolite (Conventional)

Na/ZSM-5 was ion-exchanged with 1 mol L^{-1} of TPABr aqueous solution for 20 h on a hot stirrer at 180 °C to replace Na^+ only on the external surface with TPA^+. The wet powder was collected by centrifuging. The washing, drying, and calcination processes were performed using the same procedures as mentioned above. This sample was named "ZSM-5-SA".

As a comparison, H^+-type zeolite (conventional) was prepared using the same procedures for the synthesis of ZSM-5-SA using 1 mol L^{-1} of NH_4Cl aqueous solution instead of 1 mol L^{-1} of TPABr aqueous solution. This sample was named "H/ZSM-5". A ZSM-5 sample containing a trace amount of H^+ throughout the crystal was prepared by ion exchange using 0.00059 mol L^{-1} NH_4Cl aqueous solution. This sample was named "ZSM-5-WA".

Characterization

XRD measurements were carried out using a PANalytical X'Pert PRO MPD diffractometer equipped with Cu Kα radiation to analyze the crystal structure of the samples. EDX spectroscopy was employed to determine the chemical composition of the samples. XPS analysis was performed using a Kratos Ultra 2 (Shimadzu, Kyoto, Japan). TEM was employed to investigate the microstructure and morphology of the samples. N_2 adsorption measurements were carried out at −196 °C using a BELSORP-Max instrument (MicrotracBel) to evaluate the microporous structure of the samples. Prior to the analysis, the samples were degassed under vacuum at 250 °C for 3 h. The acidic properties of the samples were characterized by NH_3 temperature-programmed desorption (NH_3-TPD) using a BELCAT II instrument equipped with a quadrupole mass spectrometer (MicrotracBEL). To comprehensively analyze the acidity of ZSM-5, FT-IR spectroscopy was conducted using pyridine as a probe molecule. Pyridine was employed to evaluate external surface acidity, as its molecular size restricts penetration into ZSM-5 micropores. Consequently, pyridine provides a reliable indicator of surface acidity. Prior to spectral measurement, pyridine-loaded samples were subjected to helium flow at 150 or 200 °C for 15 min to desorb loosely bound species.[40,41] NMR measurements were performed using AVANCE III (Bruker).

Polyethylene Catalytic Cracking

The catalytic activity of the synthesized materials was assessed via the catalytic cracking of LDPE or HDPE using TG conducted on a DTG-60A instrument (Shimadzu). LDPE (particle size: 500 μm, density: 0.94 g cm^{-3}) was supplied by Thermo Fisher Scientific. HDPE with particle size: 150 μm was used. A physical mixture of catalyst and LDPE (mass ratio = 1:4), as well as pure LDPE, was placed in alumina cells for measurement. The cracking of LDPE during heating resulted in a gradual mass loss due to gasification. The temperature at which 50% of the LDPE mass was lost (Thalf) was defined as an indicator of catalytic performance.

The volatile cracking products were collected using a gas sampling bag connected to a cold trap maintained at 0 °C with ice water. The increase in trap mass after reaction was interpreted as the yield of solid and liquid products (YS + L), calculated on a mass basis. Coke deposition on the catalyst was determined by TG under an air atmosphere with a heating rate of 5 °C min^{-1}, and the yield of coke (YC) was calculated from the weight loss between 300 and 600 °C. The gas-phase product yield (YG) was calculated as follows: YG = 100—(YS + L + YC). The gas composition was analyzed using a GC-2025 gas chromatograph (Shimadzu) equipped with a flame ionization detector.

Conflict of Interest

The authors declare no conflict of interest.

Author Contributions

Ryuga Nakai: conceptualization (lead); data curation (lead); investigation (lead); methodology (equal); writing—original draft (lead). **Shinya Kokuryo**: conceptualization (lead); investigation (supporting); methodology (lead); validation (lead); visualization (lead); writing—original draft (supporting). **Koji Miyake**: conceptualization (lead); investigation (supporting); methodology (lead); supervision (lead); validation (lead); visualization (lead); writing—review & editing (lead). **Yoshiki Murata**: investigation (supporting); methodology (supporting); writing—review & editing (supporting). **Yoshiaki Uchida**: methodology (supporting); supervision (supporting); writing—review & editing (equal). **Atsushi Mizusawa**: methodology (supporting); writing—review & editing (supporting). **Tadashi Kubo**: funding acquisition (supporting); writing—review & editing (supporting). **Norikazu Nishiyama**:

conceptualization (equal); resources (lead); supervision (lead); validation (equal); writing—review & editing (equal).

Data Availability Statement

The data that support the findings of this study are available from the corresponding author upon reasonable request.

Keywords: Brønsted acid · catalytic cracking · ion exchange · polyolefin · zeolites

[1] T. Thiounn, R. C. Smith, *J. Polym. Sci.* **2020**, *58*, 1347.
[2] F. Sasse, G. Emig, *Chem. Eng. Technol.* **1998**, *21*, 777.
[3] H. Luo, H. Tyrrell, J. Bai, R. I. Muazu, X. Long, *Green Chem.* **2024**, *26*, 11444.
[4] X. Wang, J. Xu, M. Zhao, W. Cui, X. Mu, X. Wang, S. Song, H. Zhang, *Chem. Synth.* **2024**, *4*, 2400132.
[5] S. M. Al-Salem, P. Lettieri, J. Baeyens, *Waste Manage.* **2009**, *29*, 2625.
[6] B. Thangaraj, Y.-K. Lee, *Fuel* **2025**, *380*, 133220.
[7] Q. Liu, J. Shang, Z. Liu, *Chin. J. Catal.* **2025**, *71*, 54.
[8] E. Pérez-Botella, S. Valencia, F. Rey, *Chem. Rev.* **2022**, *122*, 17647.
[9] U. M. Jibreel, A. S. Bayero, M. I. Mohamaed, B. A. Muzakkari, *IJCA* **2024**, *7*, 82.
[10] W.-H. Chen, P. P. Biswas, E. E. Kwon, Y.-K. Park, S. Rajendran, L. Gnanasekaran, J.-S. Chang, *Chem. Eng. J.* **2023**, *471*, 144695.
[11] L. Dai, N. Zhou, K. Cobb, P. Chen, Y. Wang, Y. Liu, R. Zou, H. Lei, B. A. Mohamed, Y. Cheng, R. Ruan, *Appl. Catal., B* **2022**, *318*, 121835.
[12] C. Schroeder, V. Siozios, C. Mück-Lichtenfeld, M. Hunger, M. R. Hansen, H. Koller, *Chem. Mater.* **2020**, *32*, 1564.
[13] A. Zachariou, A. P. Hawkins, R. F. Howe, J. M. S. Skakle, N. Barrow, P. Collier, D. W. Nye, R. I. Smith, G. B. G. Stenning, S. F. Parker, D. Lennon, *ACS Phys. Chem. Au* **2023**, *3*, 74.
[14] B. Xu, C. Sievers, S. B. Hong, R. Prins, J. A. van Bokhoven, *J. Catal.* **2006**, *244*, 163.
[15] M. U. Azam, W. Afzal, I. Graça, *Catalysts* **2024**, *14*, 450.
[16] G. Manos, A. Garforth, J. Dwyer, *Ind. Eng. Chem. Res.* **2000**, *39*, 1203.
[17] J. H. van de Minkelis, A. H. Hergesell, J. C. van der Waal, R. M. Altink, I. Vollmer, B. M. Weckhuysen, *ChemSusChem* **2025**, *18*, e202401141.
[18] Z. Linxi, G. Kuiqi, *Eur. Polym. J.* **1993**, *29*, 1631.
[19] M. U. Azam, A. Fernandes, M. João Ferreira, A. J. McCue, I. Graça, W. Afzal, *Fuel* **2025**, *379*, 132990.
[20] S. Tsubota, S. Kokuryo, K. Miyake, Y. Uchida, A. Mizusawa, T. Kubo, N. Nishiyama, *ACS Catal.* **2024**, *14*, 18145.
[21] V. Daligaux, R. Richard, M.-H. Manero, *Catalysts* **2021**, *11*, 770.
[22] S. Rejman, Z. M. Reverdy, Z. Bör, J. N. Louwen, C. Rieg, J. M. Dorresteijn, J.-K. van der Waal, E. T. C. Vogt, I. Vollmer, B. M. Weckhuysen, *Nat. Commun.* **2025**, *16*, 2980.
[23] X. Yang, B. Gao, W. Li, K. Hou, K. Yan, T. Yan, S. Wang, Y. Zhang, L. Wang, Y. Tang, *Chem Catal.* **2024**, *4*, 100947.
[24] S. Rejman, I. Vollmer, M. J. Werny, E. T. C. Vogt, F. Meirer, B. M. Weckhuysen, *Chem. Sci.* **2023**, *14*, 10068.
[25] Y. Wang, Y. Zhang, H. Fan, P. Wu, M. Liu, X. Li, J. Yang, C. Liu, P. Bai, Z. Yan, *Catal. Today* **2022**, *405–406*, 135.
[26] L. Yu, C. Xu, Q. Zhou, X. Fu, Y. Liang, W. Wang, *J. Alloys Compd.* **2023**, *965*, 171454.
[27] A. Coelho, L. Costa, M. M. Marques, I. M. Fonseca, M. A. N. D. A. Lemos, F. Lemos, *Appl. Catal., A* **2012**, *413*, 183.
[28] E. J. Nilsson, V. Alfredsson, D. T. Bowron, K. J. Edler, *Phys. Chem. Chem. Phys.* **2016**, *18*, 11193.
[29] H. Van Koningsveld, H. Van Bekkum, J. C. Jansen, *Acta Crystallogr., Sect. B: Struct. Sci.* **1987**, *43*, 127.
[30] M. Briend, A. Lamy, M.-J. Peltre, P. P. Man, D. Barthomeuf, *Zeolites* **1993**, *13*, 201.
[31] P. A. Jacobs, J. A. Martens, in *Studies in Surface Science and Catalysis*, Vol. *33*, Elsevier **1987**, 47–111.
[32] T. Ikeda, T. Yasunaga, *J. Colloid Interface Sci.* **1984**, *99*, 183.
[33] C. Auepattana-aumrung, K. Suriye, B. Jongsomjit, J. Panpranot, P. Praserthdam, *Catal. Today* **2020**, *358*, 237.
[34] G. Bagnasco, *J. Catal.* **1996**, *159*, 249.
[35] M. Takeuchi, T. Tsukamoto, A. Kondo, M. Matsuoka, *Catal. Sci. Technol.* **2015**, *5*, 4587.
[36] M. Niwa, N. Katada, *Chem. Rec.* **2013**, *13*, 432.
[37] V. Zholobenko, C. Freitas, M. Jendrlin, P. Bazin, A. Travert, F. Thibault-Starzyk, *J. Catal.* **2020**, *385*, 52.
[38] D. Hartanto, L. S. Yuan, S. M. Sari, D. Sugiarso, I. K. Murwarni, T. Ersam, D. Prasetyoko, H. Nur, *J. Teknol.* **2016**, *78*, 223.
[39] R. Feng, X. Yan, X. Hu, Y. Wang, Z. Li, K. Hou, J. Lin, *J. Porous Mater.* **2018**, *25*, 1743.
[40] J. Přech, P. Pizarro, D. P. Serrano, J. řejka, *Chem. Soc. Rev.* **2018**, *47*, 8263.
[41] J. Weitkamp, *Solid State Ionics* **2000**, *131*, 175.
[42] H. Bludau, H. G. Karge, W. Niessen, *Microporous Mesoporous Mater.* **1998**, *22*, 297.
[43] R. Gounder, E. Iglesia, *J. Catal.* **2011**, *277*, 36.
[44] P. M. Kester, E. Iglesia, R. Gounder, *J. Phys. Chem. C* **2020**, *124*, 15839.
[45] J. Wristers, *J. Am. Chem. Soc.* **1975**, *97*, 4312.
[46] V. Daligaux, R. Richard, M. Marin-Gallego, V. Ruaux, L. Pinard, M.-H. Manero, *Appl. Catal., A* **2024**, *671*, 119581.
[47] T. Liu, Y. Li, Y. Zhou, S. Deng, H. Zhang, *Catalysts* **2023**, *13*, 382.
[48] P. Castaño, G. Elordi, M. Olazar, A. T. Aguayo, B. Pawelec, J. Bilbao, *Appl. Catal., B* **2011**, *104*, 91.
[49] Z. Dong, W. Chen, K. Xu, Y. Liu, J. Wu, F. Zhang, *ACS Catal.* **2022**, *12*, 14882.
[50] M. N. Mazar, S. Al-Hashimi, M. Cococcioni, A. Bhan, *J. Phys. Chem. C* **2013**, *117*, 23609.
[51] W. Wang, C. Yao, X. Ge, X. Pu, J. Yuan, W. Sun, W. Chen, X. Feng, G. Qian, X. Duan, Y. Cao, Z. Yang, X. Zhou, J. Zhang, *J. Mater. Chem. A* **2023**, *11*, 14933.

Manuscript received: December 1, 2025
Version of record online: